

Learning Depth from Monocular Videos Using Synthetic Data: A Temporally-Consistent Domain Adaptation Approach

Yipeng Mou¹ Mingming Gong^{2,3} Huan Fu¹ Kayhan Batmanghelich² Kun Zhang³ Dacheng Tao¹

¹UBTECH Sydney AI Centre, SIT, FEIT, The University of Sydney, Australia

²Department of Biomedical Informatics, University of Pittsburgh

³Department of Philosophy, Carnegie Mellon University

{ymou5942@uni., hufu6371@uni, dacheng.tao@}sydney.edu.au {mig73@, kayhan@}pitt.edu kunz1@cmu.edu

Abstract

Majority of state-of-the-art monocular depth estimation methods are supervised learning approaches. The success of such approaches heavily depends on the high-quality depth labels which are expensive to obtain. Some recent methods try to learn depth networks by leveraging unsupervised cues from monocular videos which are easier to acquire but less reliable. In this paper, we propose to resolve this dilemma by transferring knowledge from synthetic videos with easily obtainable ground-truth depth labels. Due to the stylish difference between synthetic and real images, we propose a temporally-consistent domain adaptation (TCDA) approach that simultaneously explores labels in the synthetic domain and temporal constraints in the videos to improve style transfer and depth prediction. Furthermore, we make use of the ground-truth optical flow and pose information in the synthetic data to learn moving mask and pose prediction networks. The learned moving masks can filter out moving regions that produces erroneous temporal constraints and the estimated poses provide better initializations for estimating temporal constraints. Experimental results demonstrate the effectiveness of our method and comparable performance against state-of-the-art.

1. Introduction

Monocular depth estimation is a fundamental problem in computer vision and 3d scene understanding. Appreciable progress has been made in recent years thanks to the deep convolutional neural networks(DCNNs) [27, 44, 38, 7, 21, 9]. However, because most of these method consider depth estimation as a supervised learning problem, they require a large amount of images labeled with ground-truth depth maps, which are expensive to acquire in practice. To address the high cost issue, recent methods have investigated unsupervised approaches from stereo image pairs by recast-

ing depth estimation as a reconstruction progress with the intermediate disparity prediction. [16, 14, 45].

Compared to stereo images, monocular videos are cheaper and even easier to obtain. Recently, several unsupervised methods that trained solely on monocular video achieved promising performance. By incorporating 3d pose estimation and depth estimation, [50, 42] warp the image to neighbor frames and minimize the photometric consistency. However, this type of methods assume a rigid scene which brings two drawbacks to the model: 1) The moving region will generate incorrect projection and introduce noisy loss. 2) Due to the lack of motion information of moving objects, predicting the depth of moving region becomes a ill-posed problem and we have no clue to solve a unique depth value. Some fully unsupervised methods proposed to solve the moving problem by attaching a optical flow branch and deduct the moving mask [30, 35]. However, their methods only mask out the noisy loss while the moving object depth is still inaccurate without the help of stereo image.

Inspired by [24], we hope to train the model with some direct supervision from single image rather than indirect clue like photometric loss. [24] made a new dataset separating frozen people from crowds because building the synthetic dataset with moving human-being and camera motion is challenging. However, when it comes to the auto-driving setup, there is plenty of well-constructed synthetic dataset where cars and camera are moving naturally. Thus, instead of building a new dataset, we adopt domain adaptation methods for extra depth information.

The synthetic datasets perfectly solve the two previous problems: First, due to the nature of synthetic data, we can easily get a ground-truth moving mask so that the model has the ability to predict the mask and remove the noisy loss induced by moving regions. Second, the synthetic data provide pixel level depth ground-truth. Thus, the model will be trained under direct supervision and gain the ability to predict the depth of moving object.

There are some previous work applying domain adaptation to depth estimation [2, 20, 49]. However, those setups are all simply transferring the image or features ignoring the fact that geometry constraints can considerably improve both the style transfer and the task network. Many works has shown that the geometry constrains can significantly improve the quality of domain adaptation and task performance [10]. In our work, we apply the geometry correspondence upon neighbor frames of transferred images and improve the quality of our performance.

In particular, to make more effective use of synthetic data, we propose a temporally-consistent domain adaptation (TCDA) approach that simultaneously explores labeled synthetic videos and monocular real videos. Our framework consists of a image translation (domain mapping) network, a depth prediction network, a moving mask prediction network, and a camera pose estimation network. The image translation network transforms the synthetic videos to real-style videos such that depth prediction network can be trained using ground-truth labels in the synthetic domain and temporal constraints in videos to reduce the structural distortion in the translation process. In addition, the moving mask prediction network uses the camera pose and optical flow information in the synthetic data. The predicted moving mask can be used to remove unreliable photometric losses for the moving pixels, which further purify the supervision information in real monocular videos. Finally, the camera pose estimation network trained on the ground-truth pose in the synthetic data can predict poses which provides better initializations for estimation of temporal constraints in real videos. The end-to-end training of image translation and depth estimation networks with the proposed losses improves the quality of translated images as well as depth estimation accuracy. We demonstrate the effectiveness of our method on the KITTI dataset [31] and the generalization performance on the Make3D dataset [40].

2. Related Work

Monocular Depth Estimation has been studied extensively over the past decade as it’s important for understanding the 3D structure of scenes from 2D images. Early approaches relied on handcrafted features and incorporated global information by exploiting probabilistic graphical models (*e.g.*, MRFs) [40, 39, 25], and nonparametric techniques [28, 19, 26]. Thanks to the development of deep convolutional neural networks (DCNNs), recent methods developed various new network architectures for supervised monocular depth estimation [8, 27, 17, 47, 36, 34, 3, 22, 38, 4]. In the seminal work, Eigen *et al.* [8] developed the first depth estimation network that models multi-scale information. Up to now, there have been lots of follow-up works [27, 22, 7, 23, 46, 44, 9] aiming at improving or extending this work in various directions. For example, the

recent work [9] cast depth estimation as ordinal regression instead of regression and obtained state-of-the-art performance on several benchmarks.

An obvious disadvantage of supervised depth estimation is the requirement of large amounts of labeled images. To reduce the labeling cost, recent approaches sought for unsupervised methods from stereo image pairs or monocular videos [45, 14, 16, 48, 50, 42]. Though these methods are termed as “unsupervised” methods, they are different from unsupervised learning because the stereo pairs or monocular videos can provide weak supervision. In specific, Garg *et al.* [14] showed that unsupervised depth estimation can be supervised by a image reconstruction loss between stereo pairs. Following Garg *et al.* [14], later works improved the way of supervision by exploiting left-right consistency [16], semi-supervised learning [21], etc. Regarding monocular videos, Zhou *et al.* [50] proposed a strategy that learns pose and depth CNN predictors by minimizing the photometric consistency between video frames during training. Wang *et al.* [42] further proposed a differentiable direct visual odometry (DDVO) approach that directly optimizes the pose and substantially boosted the depth prediction accuracy.

Domain Adaptation aims to address the distribution shift issue such that model trained on a dataset can be generalized to a different but related dataset [33]. A large body of recent works tried to learn a domain-invariant representation via DCNNs [12, 13, 29, 1, 41]. These methods rely on various distance discrepancy measures as objective functions to match representation distributions; typical ones include maximum mean discrepancy (MMD) [29], separability measured by classifiers [13], and optimal transport [5, 6].

Coming to DA for depth estimation, Atapour *et al.* [2] developed a two-stage method which first learned a image translator [51] to stylize the real images into synthetic images, and then trained a supervised depth estimation network using the original synthetic images. Kundu *et al.* [20] proposed a content congruent regularization method to address the model collapse problem which usually happens in high-dimensional data. Recently, Zheng *et al.* [49] developed an end-to-end adaptation network, *i.e.* T²Net, where the translation network and the depth estimation network are optimized jointly so that they can improve each other. However, these works overlooked the temporal constraints from both synthetic and real domain monocular videos , thus produced unsatisfactory image translation quality.

3. Proposed Method

In this section, we will first take a brief review of how to estimate depth from monocular videos. Then we further claim our motivation based on an observation from a small experiment. Finally we will present the proposed depth estimation framework in detail.

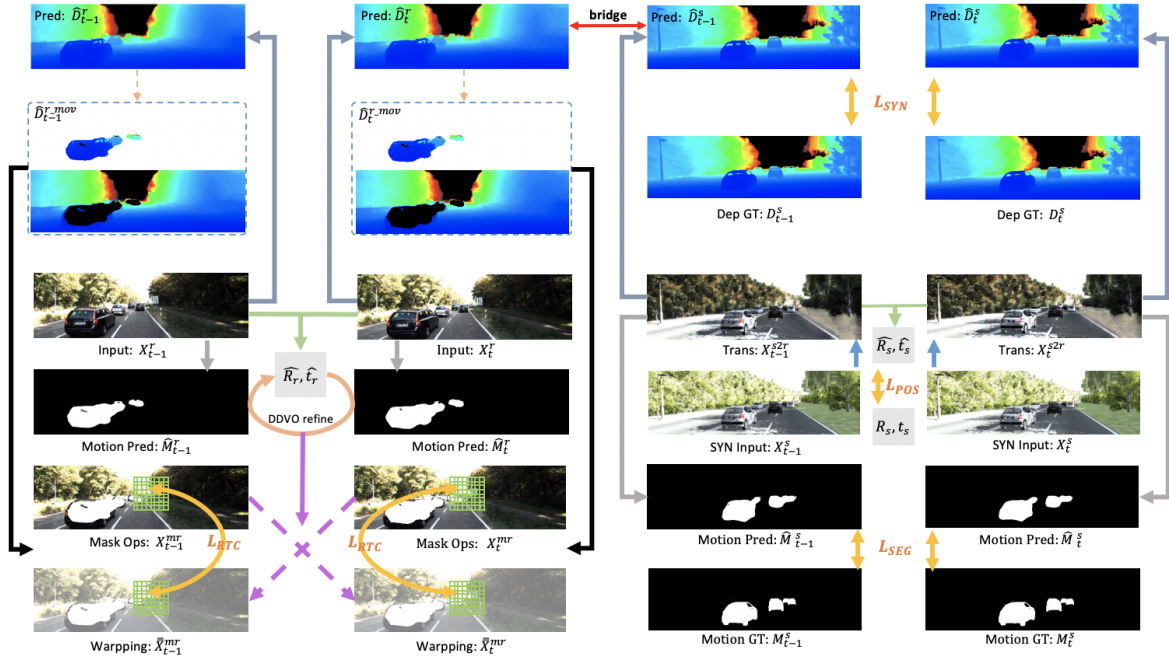


Figure 1. The proposed task network. Our model consists of three parts: a depth, a moving mask, and a relative camera pose predictor. They share the same feature from encoder E and have three different task decoder branches. p_{pred} represents the relative pose from x_t to x_{t+1} predicted by our pose estimation network.

3.1. Motivation

The goal here is to recover depth from monocular videos in an unsupervised fashion. A straightforward idea is to recast depth estimation as a reconstruction problem by modeling the temporal consistency across neighbored frames. Mathematically, let p_t denotes the positions of a single pixel of frame t , the position of the corresponding pixel in $t+1$ can be computed as $p_{t+1} = K T_{(t,t+1)} D_t(p_t) K^{-1} p_t$, where K and T represent the camera poses, D is the depth map. Thus, we can give indirect supervisions to both a camera pose network and a depth estimation network iteratively via a photometric loss on warping image.

As suggested by the above literature review, solid DE from MVs relies on accurate camera pose estimation and the robustness of the photometric constraint. Unluckily, practical dynamic scenes may contain many objects with irregular movement, which would significantly degrade the performance for both of them. In fact, even with relatively reliable camera pose [42], it is not authentic to directly enforce photometric consistency on moving regions. To alleviate this issue, several works [30, 35] exploited the to predict non-rigid and rigid moving (displacement caused by camera moving respectively), and (softly) mask out real moving regions when computing photometric loss. However, while removing noises (real moving objects) would naturally achieve more accurate depth estimation on rigid re-

gions, these approaches do not perform well on non-rigid moving regions due to lack of extra supervisions on these removed moving regions. To provide a clearer illustration, we examined our observation on ApolloScope dataset [43] via an experiment. Taking the algorithm presented in [50] as an example, we train two models with one optimized by masked (using ground truth moving masks) photometric and SSIM losses (Robust-SfMLearner), and the other one the vanilla version (SfMLearner). Specifically, from the reported scores in Table 1, both the consistent improvement on rigid regions and the degraded performance on non-rigid regions further support our analysis before. Importantly, we observe that lots of predicted depth values for moving cars is extremely large in both versions of the experiments. One of the main reasons is that vehicles have similar moving trend in both direction and speed as the cameras, which results in small disparity (i.e., large depth) estimation between neighbored frames without extra supervisions on these real moving regions. Motivated by the observations, we proposed to exploit indirect supervisions for moving regions and improve the robustness of photometric loss for depth estimation by introducing synthetic benchmarks and employing domain adaptation techniques. In the following, we will first present the overall architecture of our novel approach to unsupervised depth estimation from monocular videos and then explain how to take fully advantage of synthetic dataset to provide a solution for the issues aforementioned.

	RMSE	
	Robust-SfMLearner	SfMLearner [50]
Static	7.3158	5.31
Moving	13.0642	12.5865
All Area	8.7741	7.1775

Table 1. An illustration experiment on ApolloScope dataset.

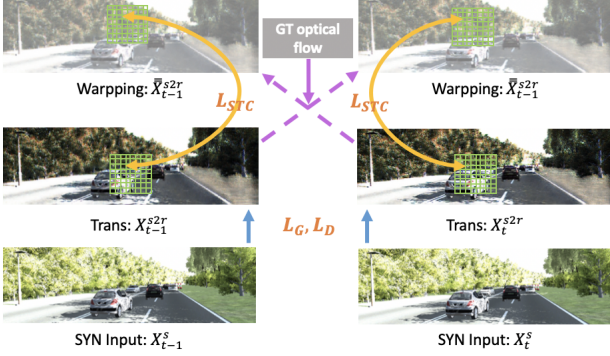


Figure 2. An illustration of the temporal consistency guided I2I translation network. Please refer Sec. 3.2.1 for details.

3.2. Overall Network Architecture

The overall network architecture, as shown in Figure 3, mainly consists of two sub-networks: 1) A temporal consistency guided image-to-image translation network which maps the images in the synthetic domain to images that have the same style as target domain, and 2) a depth prediction network that is driven by ground truth labels in synthetic domain and robust temporal constraints building on the real-domain videos. Note that, the intermediate predictions from source domain including moving masks and camera pose coupled with the domain adaptation techniques are significant to formulate reliable unsupervised constraints for target domains as analyzed before. Here, we will clearly introduce the two parts, respectively. More implementation details are provided in the supplemental materials.

3.2.1 Temporal Consistency Guided I2I Translation

To make better use of the synthetic data for depth estimation, an essential issue is how to reduce the discrepancy between synthetic domain and real domain. Previous works [2] prefer to employ CycleGAN [52], an unsupervised image-to-image translation approach, to provide a partial solution by translating synthetic images to having the same style as real images while preserving the semantic structures. However, one of the main disadvantages is that learning CycleGAN is memory intensive due to the two-directional translation strategies, which makes it not possible to train a deep domain adaptation dense prediction net-

work in an end-to-end fashion [18]. Instead, we suggest that learning an one-sided mapping by enforcing a simple but effective optical flow guided temporal consistency loss is sufficient to generate reasonable translations in our task. In fact, the supervised depth prediction branch in the synthetic domain could also prevent mode collapse and semantic distortions in a way.

Mathematically, given two successive frames x_t^s and x_{t+1}^s in the synthetic video, the translation network G maps the synthetic frames to $G(x_t^s)$ and $G(x_{t+1}^s)$. Our I2I translation networks are optimized by three objectives.

Adversarial constraint The first item is the standard adversarial loss used in GAN:

$$L_{GAN}(G, D) = \mathbb{E}_{x^r \sim P_R(x^r)} [\log(D(x^r))] + \mathbb{E}_{x^s \sim P_S(x^s)} [\log(1 - D(G(x^s)))], \quad (1)$$

where D is a discriminator network, x^r denotes real images, and P_R and P_S represent the probability distributions of real and synthetic images, respectively. Here, we consider each frame independently by ignoring the temporal relations.

Flow Guided Synthetic Temporal Consistency The second objective is the temporal consistency loss designed according to the geometric relations between the two input synthetic frames:

$$L_{STC}(G) = \mathbb{E}_{x_t^s, x_{t+1}^s \sim P_S(x_t^s, x_{t+1}^s)} [\|F(G(x_t^s)) - G(x_{t+1}^s)\|_1], \quad (2)$$

where $F(\cdot)$ is a function warping an image based on the optical flow. This loss could preserve that geometric relations between the translated images.

Identity constraint The last constraint is a widely used identity loss that stabilizes the translation process [49, 52]. The identity loss is defined as

$$L_I = \mathbb{E}_{x^r \sim P_R(x^r)} [\|G(x^r) - x^r\|_1], \quad (3)$$

which forces the translator G to be an identity mapping w.r.t. real domain images.

3.2.2 Robust Depth Prediction

Our depth prediction network follows a standard encoder-decoder structure as previously [37]. The network parameters are jointly optimized by a supervised L1 loss with image-depth pairs provided by synthetic domain, and an unsupervised robust photometric loss according to adapted camera pose and moving masks in real domain.

We indicate that the synthetic domain provides various easily captured ground truth labels (e.g., depth, segmentation, optical flow, and camera pose) but low quality translated images, while the real domain contains high quality images but unreliable photometric losses due to moving objects in the scene. Thus, as analyzed in Sec. 3.1, exploiting the complementary between each other reasonably would definitely improve the depth prediction accuracy. We will detail the jointly learning strategy of our novel robust depth prediction network.

Depth Regression Optimizing the depth prediction model in synthetic domain is straightforward. Since we are offered ground truth depth labels for each image, we directly employ L1 loss to measure the depth prediction error:

$$L_{SYN}(E, D_d, G) = \mathbb{E}_{(x^s, d_{gt}^s) \sim P_S(x^s, d_{gt}^s)} [\|D_d(E(G(x^s))) - d_{gt}^s\|_1], \quad (4)$$

where E represents the encoder which is shared by all following sub-tasks, D_d denotes the depth decoder. Note that, this branch can give direct supervision for moving regions, thus provide a remedy to the issue coming from masked photometric loss.

Camera Pose Prediction As explained in Sec. 3.1, the temporal photometric loss is sensitive to the estimation of camera poses. To provide a better initialization, we propose to learn a pose prediction network from the translated synthetic data. In specific, we take the features extracted by the encoder E from translated images as inputs and map the features to pose parameters \mathbf{p} using a pose prediction network D_p . The pose prediction network is driven by a standard L_1 loss. Note that, We also employ the differentiable direct visual odometry (DDVO) method [42] to refine the estimated camera pose during the training procedure.

Moving detection In addition, we need to perform moving detection to formulate a moving robust photometric loss. Previous works prefer to estimate optical flow to model irregular movements [30, 35]. However, on the one hand, obtaining dense flow annotations for real videos is as expensive as capturing depth annotations. On the other hand, there is still a large gap between supervised and unsupervised optical flow estimation. Here, we propose a potential solution by building a bridge between synthetic domain and real domain. In specific, we first recast moving detection as a segmentation task by generating moving mask ground truth according to the provided ground truth labels in synthetic data, i.e., optical flow, instance segmentation, camera extrinsic parameters ¹. Then, we adopt the aforementioned domain adaptation technique to handle moving

¹It is convenient for synthetic data to offer various ground truth labels.

in real videos. As a result, the loss function for the moving detection branch is expressed as:

$$L_{SEG}(M) = \mathbb{E}_{(x^s, m_{gt}^s) \sim P_S(x^s, m_{gt}^s)} [\|m_{gt} * \log(M(G(x^s)))\|_1] \quad (5)$$

Temporal Photometric Consistency Given the successive frames x_t^r and x_{t+1}^r from monocular videos, we perform indirect supervision to the depth prediction network by modeling temporal photometric consistency as previously [42]. However, the standard photometric loss in DVO is sensitive to moving objects which violates the temporal consistency as analysed before. To provide a partial remedy, we propose to consider the moving prior when computing the photometric loss. In other words, we predict moving masks via DA techniques, and develop a robust photometric constraint by ignoring the moving objects. Note that, we have extra supervisions from synthetic domain for these moving regions, thereby the issue (unreliable depth estimation for moving regions) caused by the robust photometric loss can also be addressed (refer to Sec. 3.1). Finally, given the predicted depth D_d , the relative camera pose \mathbf{p}_t^r , and estimated moving masks $M_{pred,t}^r$ and $M_{pred,t+1}^r$ for frames t -th and $t + 1$ -th, the robust temporal consistency loss is defined as:

$$L_{RTC}(\mathbf{p}_t^r, D_d, E, G) = \mathbb{E}_{x_t^r, x_{t+1}^r \sim P_R(x_t^r, x_{t+1}^r)} \|\mathcal{W}(M_{pred,t}^r \circ x_t^r, \mathbf{p}_t^r, D_d(E(G(x_t^r))) - M_{pred,t+1}^r \circ x_{t+1}^r)\|^2, \quad (6)$$

where \circ denotes element-wise product, \mathcal{W} is a warping function that maps x_t to x_{t+1} according to the estimated depth and camera pose.

4. Experiments

In this section, we first present the implementation details including the network architectures, the data-preprocessing methods, and the training/inference strategies. Then we demonstrate the effectiveness of our model on two well-known and challenging benchmarks (i.e., KITTI[15] and Make3D [39, 40]) by making a comparison with the baselines and previous state-of-the-art approaches. Finally, we perform various ablation experiments to comprehensively study the behavior of our method.

4.1. Implementation Details

Network Architecture The proposed model mainly consists of a style transfer module and a depth prediction module. For the style transfer module, we used the network architectures from T2Net [49] and remove the feature GAN part. The depth prediction module is composed of three

Method	Dataset	Supervised	Error Metrics				Accuracy Metrics		
			Abs Rel	Sq rel	RMSE	RMSE log	$\sigma < 1.25$	$\sigma < 1.25^2$	$\sigma < 1.25^3$
depth capped at 80m									
Eigen <i>et al.</i> [7]	K	Yes	0.203	1.548	6.307	0.282	0.702	0.890	0.958
Godard <i>et al.</i> [16]	K	No	0.148	1.344	5.927	0.247	0.803	0.922	0.964
DDVO [42]	K	No	0.151	1.257	5.583	0.228	0.810	0.936	0.974
Zhou <i>et al.</i> [50]	K	No	0.208	1.768	6.856	0.283	0.678	0.885	0.957
Kundu <i>et al.</i> [32]	K+V	No	0.214	1.932	7.157	0.295	0.665	0.882	0.950
Kundu <i>et al.</i> [32]	K+V	semi	0.167	1.257	5.578	0.237	0.771	0.922	0.971
Zheng <i>et al.</i> [49]	K+V	No	0.174	1.410	6.046	0.253	0.754	0.916	0.966
Sensitive-TCDA	K+V	No	0.155	1.144	5.578	0.229	0.794	0.931	0.974
TCDA	K+V	No	0.145	1.058	5.291	0.215	0.816	0.941	0.977
depth capped at 50m									
Garg[14]	K	No	0.169	1.080	5.104	0.273	0.740	0.904	0.962
Kundu <i>et al.</i> [32]	K+V	No	0.203	1.734	6.251	0.284	0.687	0.899	0.958
Kundu <i>et al.</i> [32]	K+V	semi	0.162	1.041	4.344	0.225	0.784	0.930	0.974
Zheng <i>et al.</i> [49]	K+V	No	0.168	1.199	4.674	0.243	0.772	0.912	0.966
Sensitive-TCDA	K+V	No	0.149	0.879	4.191	0.216	0.806	0.940	0.978
TCDA	K+V	No	0.139	0.814	3.995	0.203	0.830	0.949	0.980

Table 2. The result is evaluated on the Eigen *et al.* [7] split of KITTI[15]. Here, K represents KITTI, V is vKITTI (synthetic dataset), and Sensitive-TCDA denotes our model with the standard photometric constraint.

Method	Train	Error Metrics (the lower the better)			
		Abs Rel	Sq Rel	RMSE	RMSE(log)
Mean	NA	0.876	13.98	12.27	0.307
Karsch <i>et al.</i> [19]	Yes	0.428	5.079	8.389	0.149
Laina <i>et al.</i> [22]	Yes	0.204	1.840	5.683	0.084
Godard <i>et al.</i> [16]	No	0.544	10.94	11.76	0.193
Zhou <i>et al.</i> [50]	No	0.383	5.321	10.47	0.478
DDVO [42]	No	0.387	4.720	8.09	0.204
Zheng <i>et al.</i> [49]	No	0.428	5.132	8.926	0.208
TCDA	No	0.384	3.885	7.645	0.181

Table 3. Performance on Make3D. The ‘‘train’’ column states whether the method is trained on make3d training set. Metrics is computed in the central image crop with depth capped at 70m.

main sub-networks including a depth estimation network, a moving detection network, and a camera pose prediction network. The structures of the former two follow UNet [37] fashion, and the development of the camera pose network is inspired by [50].

Data Pre-processing We perform the proposed TCDA method by employing vKITTI (labeled) as the source domain and KITTI (unlabeled) as the target domain. We collect 40000 and 12000 pairs of neighbor frames from KITTI and vKITTI, respectively. The images are then resized to 192×640 in both our training and inference stages.

In our setting, while several kinds of ground truth labels (i.e., moving mask, camera pose, and depth) are accessible for vKITTI images, KITTI can only provide some video sequences. We normalize the ground truth depth from [0, 80] to [-1, 1]. The pixels with depth greater than 80m are

labeled as 1 in our training stage.

Training strategy As aforementioned, our model deeply relies on generative adversarial networks. However, the training of GANs is currently known to be unstable. Thus, we cannot directly optimize the whole framework in an end-to-end fashion from scratch. Instead, we pre-train the naive depth adaptation model which only contains a style transfer network and a depth adaptation network (i.e., the left part in Figure 2). Then, we train the camera pose network and the moving detection network for some epochs using the translated images by freezing the parameters that were obtained in the previous stage. Finally, we introduce the DDVO block and fine-tune the whole framework in an end-to-end manner. Note that, the pre-training stages can offer a relatively robust initialization to prevent the model from generating unreasonable translations and depth predictions caused by the instability of GANs.

4.2. Benchmark performance: KITTI

As done previously, we evaluate our method on the KITTI Eigen split (697 images) at the distances of 80m and 50m, respectively. The evaluation codes and the center cropping strategies are provided by [50]. The scores are reported in Table 2. Our method outperforms previous UDA approaches [49, 2, 20] and previous monocular video approaches [50, 42] by a convincing margin. Importantly, our model yields higher scores than previous state-of-the-art DDVO [42] (video depth estimation algorithm) due to our two aspects of refinement of photometric loss. We also make qualitative comparisons with DDVO [42]. As shown

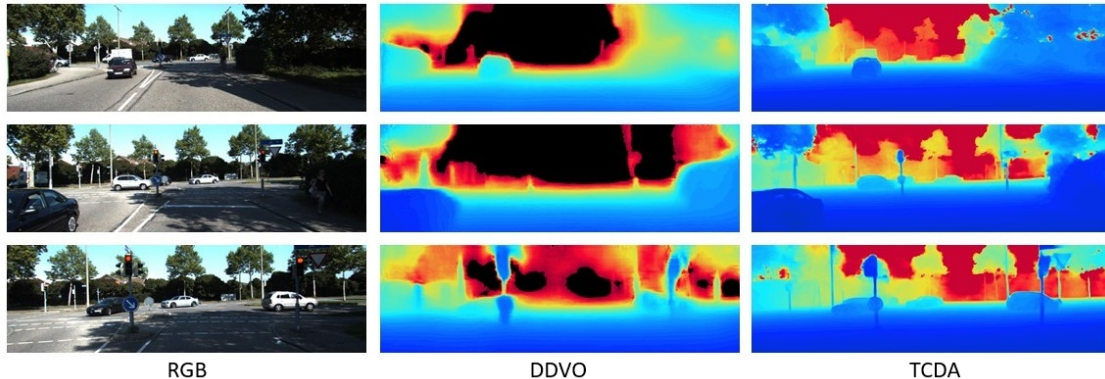


Figure 3. Dynamic scene outcome: The qualitative comparison between DDVO [42] and our TCDA.

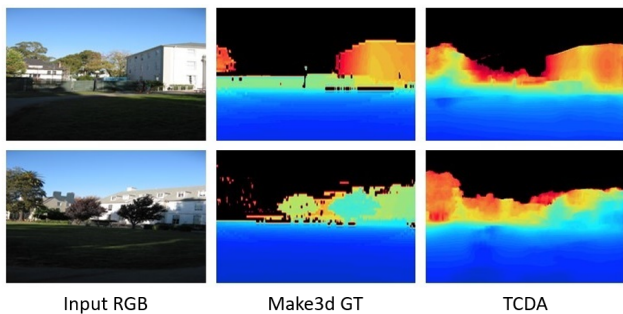


Figure 4. Qualitative Result on Make3D dataset. The groundtruth is interpolated for demonstration.

in Figure 3, DDVO cannot identify the moving cars around the traffic light. In contrast, our model can recognize most of the moving vehicles. In addition, the outlines of objects are preserved in our method, while DDVO often produces blurry outputs.

4.3. Benchmark performance: Make3D

We study the generalization capability of our model on the Make3D [39, 40] test dataset. The scores are reported in Table 3. Despite the large domain shift between KITTI and Make3D, our method can still produce reasonable predictions, and generally performs better than previous state-of-the-art methods. Note that, the evaluated model is not trained or fine-tuned using the Make3D images. Some qualitative results are shown in Figure 4.

5. Ablation Study

To further analyze our method, we conduct several ablation studies to discuss each part of our structure and demonstrate their outcomes. We evaluate these variants on the KITTI test set and report the scores in Table 4.

5.1. Robust Photometric Constraint

We demonstrate that standard photometric loss is sensitive to moving regions. We take a conventional SFM based depth estimation network [50] as an example, and perform SFM and Robust-SFM respectively. Here, Robust-SFM represents SFM driven by the robust photometric loss, where the moving regions are masked out. We pre-compute the moving masks according to the pre-trained moving detector network of TCDA. From the scores reported in Table 4, moving guided photometric loss can significantly improve SFM by a large margin

5.2. Domain Adaptation

We then study the importance of domain adaptation by making a comparison between No_DA and UDA. Here, No_DA represents the model that is directly trained via synthetic images without adaptation and corresponding ground truth depth maps provided by vKITTI. UDA is the naive domain adaptation model which is optimized the GAN loss (1), the Identity loss (3), and the synthetic depth loss(4). As shown in Table 4, No_DA performs badly on real images (target domain) due to the large domain shift between vKITTI and KITTI, while UDA provides an effective remedy to this issue.

5.3. Temporal Consistency

We investigate the effectiveness of temporal consistency losses by examining TCDA together with two variants including UDA and DA-RTC. In specific, we formulate DA-RTC by integrating the real temporal consistency loss (6) into the aforementioned UDA model. We can see from Table 4 that applying both L_{RTC} (DA-RTC v.s. UDA) and L_{STC} (TCDA v.s. DA-RTC) would yield remarkable improvements over baselines. Qualitative comparisons will be provided in the supplementary material.

	Method	Error metric				Accuracy metric		
		Abs Rel	Sq Rel	RMSE	RMSE log	$\sigma < 1.25$	$\sigma < 1.25^2$	$\sigma < 1.25^3$
SFM	SFM	0.272	1.793	5.048	0.288	0.652	0.888	0.957
	Robust-SFM	0.165	1.004	4.795	0.231	0.770	0.929	0.975
DA	NO_DA	0.284	2.459	6.816	0.382	0.508	0.780	0.907
	UDA	0.172	1.191	4.741	0.250	0.765	0.910	0.965
	DA-RTC	0.161	0.997	4.208	0.223	0.798	0.932	0.974
	Sensitive-TCDA	0.149	0.879	4.191	0.216	0.806	0.940	0.978
	TCDA (DA-RTC-STC)	0.139	0.814	3.995	0.203	0.830	0.949	0.980

Table 4. The results of different ablation study we conducted. The performance is evaluated on KITTI Eigen split and the depth is capped at 50m. STC stands for synthetic temporal consistency, RTC denotes real temporal consistency. We first compare Robust-SFM and SFM where the photometric constraint are refined or not refined by moving masks. Then we introduce the DA methods: NO_DA represents model without translation network, UDA is vanilla domain adaptation method. DA-RTC stands for only applying the temporal consistency upon real domain. Sensitive-TCDA is TCDA trained with standard photometric loss.

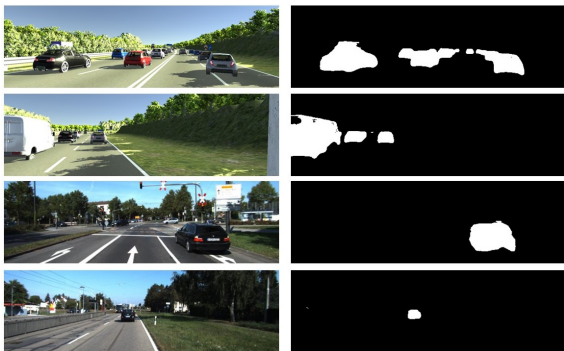


Figure 5. Moving mask predictions on vKITTI and KITTI dataset. The first and second images on the left column are samples from synthetic domain (vKITTI). The third and fourth images on the left column are samples from real domain (KITTI). The corresponding moving masks are shown in the right column.

5.4. Moving Mask

The camera pose modular and photometric loss are sensitive to dynamic scenes where objects show irregular movements. Thus, we propose to integrate moving detection to revise the photometric loss, expecting to improve both the camera pose estimation network and the translation network. The moving objects of vKITTI and KITTI are not diverse, but commonly some cars with regular moving trends. However, training TCDA with the guided moving information still improves the performance as shown in Table 4 (Sensitive-TCDA v.s. TCDA). Thereby, we believe that the moving mask detection component would show significance in complex scenes with unconstrained moving objects. The failure cases in Figure 6 also support our analysis. In specific, vKITTI (source domain) does not contain scenes with pedestrians, which degrading the performance of the moving object detection network in recognizing moving pedestrians in target domain. As a result, the depth map misses the person details in some regions.

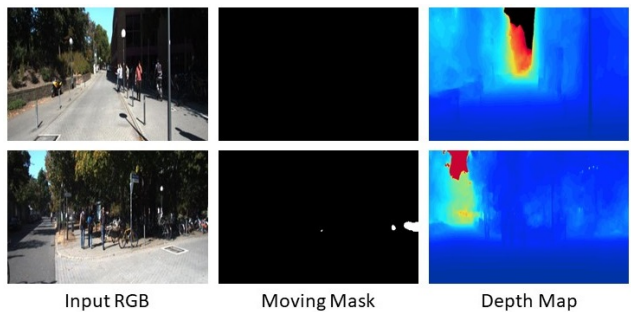


Figure 6. Failure cases. Our model failed on the scene with lots of pedestrians, because there is no pedestrian appearing in the vKITTI [11] dataset.

6. Conclusion

In the paper, we have proposed a temporally-consistent domain adaptation (TCDA) approach to deeply explore the labeled synthetic videos and monocular real videos for monocular depth estimation. We demonstrated that the temporal geometry consistency constraints in both synthetic and real videos play an important role in improving the performance of domain adaptation by improving the quality of translated images as well as the overall depth prediction accuracy. Furthermore, given that the temporal consistency in real videos guided by camera pose and depth is sensitive to the moving objects in the scene, we further proposed a moving mask prediction network trained using synthetic data, which can mask out the moving pixels and thus remove the outlier points in the temporal consistency in real videos. Finally, we proposed to train a camera pose prediction network from synthetic data with camera pose ground truth, which can provide better initialization for estimating the temporal consistency. The deep exploration of synthetic data significantly boosts the effectiveness of domain adaptation and the final depth prediction performance.

References

- [1] Hana Ajakan, Pascal Germain, Hugo Larochelle, François Laviolette, and Mario Marchand. Domain-adversarial neural networks. *arXiv preprint arXiv:1412.4446*, 2014. [2](#)
- [2] Amir Atapour-Abarghouei and Toby P Breckon. Real-time monocular depth estimation using synthetic data with domain adaptation via image style transfer. In *Proceedings of the IEEE Conference on Computer Vision and Pattern Recognition*, volume 18, page 1, 2018. [2](#), [4](#), [6](#)
- [3] Yuanzhouhan Cao, Zifeng Wu, and Chunhua Shen. Estimating depth from monocular images as classification using deep fully convolutional residual networks. *arXiv preprint arXiv:1605.02305*, 2016. [2](#)
- [4] Weifeng Chen, Zhao Fu, Dawei Yang, and Jia Deng. Single-image depth perception in the wild. In *Advances in Neural Information Processing Systems*, pages 730–738, 2016. [2](#)
- [5] Nicolas Courty, Rémi Flamary, Devis Tuia, and Alain Rakotomamonjy. Optimal transport for domain adaptation. *IEEE transactions on pattern analysis and machine intelligence*, 39(9):1853–1865, 2017. [2](#)
- [6] Bharath Bhushan Damodaran, Benjamin Kellenberger, Rémi Flamary, Devis Tuia, and Nicolas Courty. Deepjdot: Deep joint distribution optimal transport for unsupervised domain adaptation. In *European Conference on Computer Vision*, pages 467–483. Springer, 2018. [2](#)
- [7] David Eigen and Rob Fergus. Predicting depth, surface normals and semantic labels with a common multi-scale convolutional architecture. In *Proceedings of the IEEE international conference on computer vision*, pages 2650–2658, 2015. [1](#), [2](#), [6](#)
- [8] David Eigen, Christian Puhrsch, and Rob Fergus. Depth map prediction from a single image using a multi-scale deep network. In *Advances in neural information processing systems*, pages 2366–2374, 2014. [2](#)
- [9] Huan Fu, Mingming Gong, Chaohui Wang, Kayhan Batmanghelich, and Dacheng Tao. Deep ordinal regression network for monocular depth estimation. In *Proceedings of the IEEE Conference on Computer Vision and Pattern Recognition*, pages 2002–2011, 2018. [1](#), [2](#)
- [10] Huan Fu, Mingming Gong, Chaohui Wang, Kayhan Batmanghelich, Kun Zhang, and Dacheng Tao. Geometry-consistent adversarial networks for one-sided unsupervised domain mapping. *arXiv preprint arXiv:1809.05852*, 2018. [2](#)
- [11] Adrien Gaidon, Qiao Wang, Yohann Cabon, and Eleonora Vig. Virtual worlds as proxy for multi-object tracking analysis. In *Proceedings of the IEEE conference on computer vision and pattern recognition*, pages 4340–4349, 2016. [8](#)
- [12] Yaroslav Ganin and Victor S. Lempitsky. Unsupervised domain adaptation by backpropagation. In *ICML*, 2015. [2](#)
- [13] Yaroslav Ganin, Evgeniya Ustinova, Hana Ajakan, Pascal Germain, Hugo Larochelle, François Laviolette, Mario Marchand, and Victor Lempitsky. Domain-adversarial training of neural networks. *The Journal of Machine Learning Research*, 17(1):2096–2030, 2016. [2](#)
- [14] Ravi Garg, Vijay Kumar BG, Gustavo Carneiro, and Ian Reid. Unsupervised cnn for single view depth estimation: Geometry to the rescue. In *European Conference on Computer Vision*, pages 740–756. Springer, 2016. [1](#), [2](#), [6](#)
- [15] Andreas Geiger, Philip Lenz, Christoph Stiller, and Raquel Urtasun. Vision meets robotics: The kitti dataset. *International Journal of Robotics Research (IJRR)*, 2013. [5](#), [6](#)
- [16] Clément Godard, Oisín Mac Aodha, and Gabriel J Brostow. Unsupervised monocular depth estimation with left-right consistency. In *Proceedings of the IEEE Conference on Computer Vision and Pattern Recognition*, pages 270–279, 2017. [1](#), [2](#), [6](#)
- [17] Lei He, Guanghui Wang, and Zhanyi Hu. Learning depth from single images with deep neural network embedding focal length. *IEEE Transactions on Image Processing*, 2018. [2](#)
- [18] Judy Hoffman, Eric Tzeng, Taesung Park, Jun-Yan Zhu, Phillip Isola, Kate Saenko, Alexei A. Efros, and Trevor Darrell. Cycada: Cycle consistent adversarial domain adaptation. In *International Conference on Machine Learning (ICML)*, 2018. [4](#)
- [19] Kevin Karsch, Ce Liu, and Sing Bing Kang. Depth transfer: Depth extraction from video using non-parametric sampling. *IEEE transactions on pattern analysis and machine intelligence*, 36(11):2144–2158, 2014. [2](#), [6](#)
- [20] Jogendra Nath Kundu, Phani Krishna Uppala, Anuj Pahuja, and R Venkatesh Babu. Adadepth: Unsupervised content congruent adaptation for depth estimation. *arXiv preprint arXiv:1803.01599*, 2018. [2](#), [6](#)
- [21] Yevhen Kuznietsov, Jorg Stuckler, and Bastian Leibe. Semi-supervised deep learning for monocular depth map prediction. In *Proceedings of the IEEE Conference on Computer Vision and Pattern Recognition*, pages 6647–6655, 2017. [1](#), [2](#)
- [22] Iro Laina, Christian Rupprecht, Vasileios Belagiannis, Federico Tombari, and Nassir Navab. Deeper depth prediction with fully convolutional residual networks. In *2016 Fourth International Conference on 3D Vision (3DV)*, pages 239–248. IEEE, 2016. [2](#), [6](#)
- [23] Bo Li, Chunhua Shen, Yuchao Dai, Anton Van Den Hengel, and Mingyi He. Depth and surface normal estimation from monocular images using regression on deep features and hierarchical crfs. In *Proceedings of the IEEE Conference on Computer Vision and Pattern Recognition*, pages 1119–1127, 2015. [2](#)
- [24] Zhengqi Li, Tali Dekel, Forrester Cole, Richard Tucker, Noah Snavely, Ce Liu, and William T Freeman. Learning the depths of moving people by watching frozen people. In *Proceedings of the IEEE Conference on Computer Vision and Pattern Recognition*, pages 4521–4530, 2019. [1](#)
- [25] Beyang Liu, Stephen Gould, and Daphne Koller. Single image depth estimation from predicted semantic labels. In *Computer Vision and Pattern Recognition (CVPR), 2010 IEEE Conference on*, pages 1253–1260. IEEE, 2010. [2](#)
- [26] Ce Liu, Jenny Yuen, and Antonio Torralba. Sift flow: Dense correspondence across scenes and its applications. *IEEE transactions on pattern analysis and machine intelligence*, 33(5):978–994, 2011. [2](#)
- [27] Fayao Liu, Chunhua Shen, Guosheng Lin, and Ian Reid. Learning depth from single monocular images using deep

- convolutional neural fields. *IEEE transactions on pattern analysis and machine intelligence*, 38(10):2024–2039, 2016. [1](#), [2](#)
- [28] Miaomiao Liu, Mathieu Salzmann, and Xuming He. Discrete-continuous depth estimation from a single image. In *Proceedings of the IEEE Conference on Computer Vision and Pattern Recognition*, pages 716–723, 2014. [2](#)
- [29] M. Long, Y. Cao, J. Wang, and M. Jordan. Learning transferable features with deep adaptation networks. In David Blei and Francis Bach, editors, *ICML*, pages 97–105. JMLR Workshop and Conference Proceedings, 2015. [2](#)
- [30] Chenxu Luo, Zhenheng Yang, Peng Wang, Yang Wang, Wei Xu, Ram Nevatia, and Alan Yuille. Every pixel counts++: Joint learning of geometry and motion with 3d holistic understanding. *arXiv preprint arXiv:1810.06125*, 2018. [1](#), [3](#), [5](#)
- [31] Moritz Menze and Andreas Geiger. Object scene flow for autonomous vehicles. In *Proceedings of the IEEE Conference on Computer Vision and Pattern Recognition*, pages 3061–3070, 2015. [2](#)
- [32] Jogendra Nath Kundu, Phani Krishna Uppala, Anuj Pahuja, and R Venkatesh Babu. Adadepth: Unsupervised content congruent adaptation for depth estimation. In *Proceedings of the IEEE Conference on Computer Vision and Pattern Recognition*, pages 2656–2665, 2018. [6](#)
- [33] Sinno Jialin Pan, Qiang Yang, et al. A survey on transfer learning. *IEEE Transactions on knowledge and data engineering*, 22(10):1345–1359, 2010. [2](#)
- [34] Xiaojuan Qi, Renjie Liao, Zhengzhe Liu, Raquel Urtasun, and Jiaya Jia. Geonet: Geometric neural network for joint depth and surface normal estimation. In *Proceedings of the IEEE Conference on Computer Vision and Pattern Recognition*, pages 283–291, 2018. [2](#)
- [35] Anurag Ranjan, Varun Jampani, Lukas Balles, Kihwan Kim, Deqing Sun, Jonas Wulff, and Michael J Black. Competitive collaboration: Joint unsupervised learning of depth, camera motion, optical flow and motion segmentation. In *Proceedings of the IEEE Conference on Computer Vision and Pattern Recognition*, pages 12240–12249, 2019. [1](#), [3](#), [5](#)
- [36] Vamshi Krishna Repala and Shiv Ram Dubey. Dual cnn models for unsupervised monocular depth estimation. *arXiv preprint arXiv:1804.06324*, 2018. [2](#)
- [37] Olaf Ronneberger, Philipp Fischer, and Thomas Brox. U-net: Convolutional networks for biomedical image segmentation. In *International Conference on Medical image computing and computer-assisted intervention*, pages 234–241. Springer, 2015. [4](#), [6](#)
- [38] Anirban Roy and Sinisa Todorovic. Monocular depth estimation using neural regression forest. In *Proceedings of the IEEE conference on computer vision and pattern recognition*, pages 5506–5514, 2016. [1](#), [2](#)
- [39] Ashutosh Saxena, Sung H Chung, and Andrew Y Ng. Learning depth from single monocular images. In *Advances in neural information processing systems*, pages 1161–1168, 2006. [2](#), [5](#), [7](#)
- [40] Ashutosh Saxena, Min Sun, and Andrew Y Ng. Make3d: Learning 3d scene structure from a single still image. *IEEE transactions on pattern analysis and machine intelligence*, 31(5):824–840, 2009. [2](#), [5](#), [7](#)
- [41] Baochen Sun and Kate Saenko. Deep coral: Correlation alignment for deep domain adaptation. In *European Conference on Computer Vision*, pages 443–450. Springer, 2016. [2](#)
- [42] Chaoyang Wang, José Miguel Buenaposada, Rui Zhu, and Simon Lucey. Learning depth from monocular videos using direct methods. In *Proceedings of the IEEE Conference on Computer Vision and Pattern Recognition*, pages 2022–2030, 2018. [1](#), [2](#), [3](#), [5](#), [6](#), [7](#)
- [43] Peng Wang, Xinyu Huang, Xinjing Cheng, Dingfu Zhou, Qichuan Geng, and Ruigang Yang. The apolloscape open dataset for autonomous driving and its application. *IEEE transactions on pattern analysis and machine intelligence*, 2019. [3](#)
- [44] Peng Wang, Xiaohui Shen, Zhe Lin, Scott Cohen, Brian Price, and Alan L Yuille. Towards unified depth and semantic prediction from a single image. In *Proceedings of the IEEE Conference on Computer Vision and Pattern Recognition*, pages 2800–2809, 2015. [1](#), [2](#)
- [45] Junyuan Xie, Ross Girshick, and Ali Farhadi. Deep3d: Fully automatic 2d-to-3d video conversion with deep convolutional neural networks. In *European Conference on Computer Vision*, pages 842–857. Springer, 2016. [1](#), [2](#)
- [46] Dan Xu, Elisa Ricci, Wanli Ouyang, Xiaogang Wang, and Nicu Sebe. Multi-scale continuous crfs as sequential deep networks for monocular depth estimation. In *Proceedings of CVPR*, volume 1, 2017. [2](#)
- [47] Dan Xu, Wei Wang, Hao Tang, Hong Liu, Nicu Sebe, and Elisa Ricci. Structured attention guided convolutional neural fields for monocular depth estimation. In *Proceedings of the IEEE Conference on Computer Vision and Pattern Recognition*, pages 3917–3925, 2018. [2](#)
- [48] Zhichao Yin and Jianping Shi. Geonet: Unsupervised learning of dense depth, optical flow and camera pose. In *Proceedings of the IEEE Conference on Computer Vision and Pattern Recognition (CVPR)*, volume 2, 2018. [2](#)
- [49] Chuanxia Zheng, Tat-Jen Cham, and Jianfei Cai. T2net: Synthetic-to-realistic translation for solving single-image depth estimation tasks. In *Proceedings of the European Conference on Computer Vision (ECCV)*, pages 767–783, 2018. [2](#), [4](#), [5](#), [6](#)
- [50] Tinghui Zhou, Matthew Brown, Noah Snavely, and David G Lowe. Unsupervised learning of depth and ego-motion from video. In *Proceedings of the IEEE Conference on Computer Vision and Pattern Recognition*, pages 1851–1858, 2017. [1](#), [2](#), [3](#), [4](#), [6](#), [7](#)
- [51] Jun-Yan Zhu, Taesung Park, Phillip Isola, and Alexei A Efros. Unpaired image-to-image translation using cycle-consistent adversarial networks. In *Proceedings of the IEEE International Conference on Computer Vision*, pages 2223–2232, 2017. [2](#)
- [52] Jun-Yan Zhu, Taesung Park, Phillip Isola, and Alexei A Efros. Unpaired image-to-image translation using cycle-consistent adversarial networks. In *Computer Vision (ICCV), 2017 IEEE International Conference on*, 2017. [4](#)